ACS APPLIED ELECTRONIC MATERIALS

pubs.acs.org/acsaelm Article

Oxide Decomposition and Sn Surface Segregation on Core/Shell Ge/GeSn Nanowires

Michael R. Braun, J. Zach Lentz, Ishaa Bishnoi, Andrew C. Meng, Lee Casalena, Huikai Cheng, and Paul C. McIntyre*

Cite This: *ACS Appl. Electron. Mater.* 2022, 4, 5406−5412 Read Online

ACCESS | Metrics & More | Article Recommendations | Supporting Information

ABSTRACT: As a direct bandgap Group IV alloy, metastable $Ge_{1-x}Sn_x$ (x > ~0.1) is an extremely interesting optical and electronic material. Germanium core/germanium-tin coaxial heterostructures offer an opportunity to study Sn surface segregation from $Ge_{1-x}Sn_x$ alloys in the technologically interesting composition range that exceeds the maximum solid solubility of tin in diamond cubic structure germanium. We investigate the annealing characteristics of the germanium-tin surface and native oxide for tin contents in the range of 2 to 12 at% for initial conditions ranging from intentional air exposure to surface oxide-free nanowires. For air-exposed samples, we show the presence of a tin-rich oxide that exhibits a composition dependent temperature for thermal decomposition during postdeposition annealing in the XPS chamber. Across the range of Sn compositions investigated, the decomposition temperatures of tin oxide and germanium oxide were found to be the same, indicating a single-phase oxide in which both components decompose simultaneously. Utilizing nominally air-free transfer of freshly synthesized and rapid thermally annealed Ge/GeSn nanowires, we investigated the effects of hydrogen and vacuum (~50 mTorr) annealing and show the inhibition of Sn segregation to the GeSn shell surface when a surface oxide forms. Formation of a surface oxide during an anneal inhibits further Sn surface segregation and, compared to hydrogen anneals, permits an approximately 175 °C increase in the annealing temperature window before changes occur in the nanowire surface morphology, thus promoting thermal stability needed for many device fabrication processes.

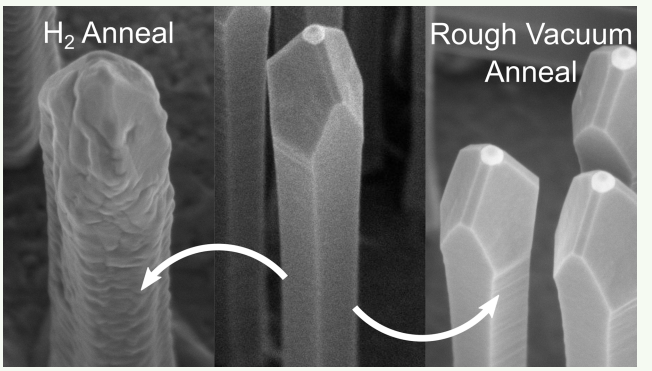

KEYWORDS: *germanium−tin, nanowires, phase segregation, in situ characterization, core/shell, surface, XPS*

INTRODUCTION

Germanium-tin alloys are increasingly investigated as Group IV semiconductors, in which a direct bandgap can be achieved in alloys with sufficiently high tin concentration. Theoretical and experimental studies have reported compositions between 6 and 10 at% Sn are required for transition to a direct bandgap, which is significantly greater than the maximum equilibrium solid solubility of Sn in Ge of ~1 at%. Synthesis via several techniques, including chemical vapor deposition (CVD), can be used to grow metastable GeSn layers with Sn contents exceeding 10 at%.[1−6] In addition to their promising optoelectronic properties, GeSn alloys, like Ge, have been investigated for application as the channel material in metal-oxide-semiconductor (MOS) field effect transistors. In particular, Ge and GeSn are promising p-type channel materials with greater hole mobilities than Si or III−V compound semiconductors.[7,8] Compared to pure Ge-based transistor channels, GeSn can provide even higher hole mobilities.[9] However, unlike silicon oxide formed in MOS gates stacks, oxides of Ge are generally defective[7] and have inferior thermal stability.[10−13] While Ge oxide stability has been well studied,[10−18] surface oxides on GeSn alloys have only had limited investigation, with prior reports focusing on plasma oxidation[6] and a 400 °C thermal oxidation[19] process.

The device performance of GeSn can be limited by both bulk and surface/interface defects, which can unintentionally dope GeSn and provide states for carrier trapping and nonradiative recombination. Vacancy defects in as-grown Ge and GeSn have been widely reported. These vacancies produce defect states at energies near the valence band edge, acting as acceptors, and cause the material to be p-type as grown.[20,21] Previous work on annealing of Ge[22] and low Sn content GeSn[23] has shown evidence of vacancy annihilation after

Received: August 16, 2022
Accepted: October 17, 2022
Published: November 1, 2022

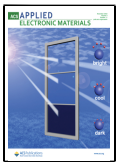

https://doi.org/10.1021/acsaelm.2c01061
ACS Appl. Electron. Mater. 2022, 4, 5406−5412

annealing at 500 °C for approximately 30 min. This annealing procedure also resulted in increased carrier mobility for GeSn samples.[23] An additional method previously utilized in Si and Ge is hydrogen annealing[24] to passivate, rather than eliminate, defects.

Due to the metastability of $Ge_{1-x}Sn_x$ alloys having technologically interesting compositions, elimination of vacancy defects via annealing has additional complexity compared to elimination of vacancy defects in pure Ge. Annealing enhances the kinetics of Sn segregation to the surface of a metastable alloy sample. Most previous reports of such phenomena utilized $Ge_{1-x}Sn_x$ thin films, which are typically either compressively strained and/or partially relaxed via formation of misfit dislocations due to the large lattice mismatch between $Ge_{1-x}Sn_x$ and typical substrates, Ge or Si. Compressive elastic strain provides a driving force for diffusion of misfitting impurity atoms to the crystal surface, and the presence of dislocations[25,26] can dramatically increase the rate of diffusion within a material, thus promoting Sn segregation. Previous reports also generally focused on air-exposed thin films, in which the initial surface composition was not well characterized. Prior annealing studies of $Ge_{1-x}Sn_x$, summarized in Table S1, have explored different environments, including H_2,[27] N_2,[2,28−32] and vacuum,[6,33−35] and various thermal budgets, with anneal times ranging from tens of seconds[28,31,36,38,39] to 2 h.[33] A general trend is observed that increased Sn content and long duration anneals cause Sn segregation even at relatively low temperatures. These reports suggest, as an approximate benchmark, that an ∼8 at% Sn alloy should exhibit measurable Sn surface segregation at 400 °C after ∼5 min. Further, these previous studies are almost exclusively on planar thin film $Ge_{1-x}Sn_x$ layers deposited on bulk substrates meaning that residual compressive elastic strains in the $Ge_{1-x}Sn_x$ films can contribute to the observed segregation behavior. Very few of these prior studies used highly surface sensitive techniques such as X-ray photoelectron spectroscopy (XPS) or Auger electron spectroscopy (AES).

Herein we report data using a nanowire core/shell geometry that minimizes the residual compressive strain[37] in the $Ge_{1-x}Sn_x$ shell to suppress the elastic energy driving force[38] for Sn segregation, which contributes in a poorly characterized manner in many of the prior reports on Sn segregation during annealing of germanium-tin thin films. The chemical state of the surface during annealing has not been well studied previously and may provide insight into nature of Sn segregation. XPS enabled examination of the behavior of the $Ge_{1-x}Sn_x$ surface oxide during annealing either during *in situ* heating inside the XPS chamber or during annealing in the rapid thermal chemical vapor deposition chamber in which the nanowires were grown. The nanowire geometry further aids the XPS measurements by increasing the available surface area within the incident X-ray spot size, thus increasing the number of emitted photoelectrons.

METHODS

Core/shell $Ge/Ge_{1-x}Sn_x$ nanowires were grown via a three-step process consisting of gold catalyzed vapor-liquid-solid (VLS) growth along with CVD deposition similar to that previously reported.[37,39−41] The deposition system used consisted of a load-locked, lamp-heated, rapid thermal, 8 in. quartz cold wall CVD chamber with a base pressure of approximately 10^{-7} Torr. Nanowires were synthesized from gold colloids (Alfa Aesar J67001) deposited by drop casting with added HF(aq) onto Sb-doped n-type Ge (111) substrates (MTI GESbc101D05C1R0014US). The source gases were germane (10% GeH_4 in H_2) as the germanium precursor and tin tetrachloride ($SnCl_4$) passively evaporated from a liquid bubbler. Hydrogen was used as a carrier gas, and all samples were grown at a constant total pressure of 30 Torr. Nanowire samples were imaged in an FEI Magellan 400 scanning electron microscope (SEM) and an FEI Helios NanoLab 600i DualBeam SEM/FIB.

X-ray photoelectron spectroscopy surface analysis was performed using a PHI VersaProbe III using a monochromated 1486 eV Al source with an *in situ* hot/cold stage and a takeoff angle of 45°. All samples were scanned with a 100 W source power over an approximately 0.1 × 1.4 mm area using the High Power (HP) mode of the instrument. A pass energy of 112 eV and energy step of 0.1 eV were used for each transition, with a variable number of repeats per transition based on signal-to-noise levels. Samples measured with the *in situ* hot/cold stage were limited to a temperature ramp rate of approximately 0.5 °C/s. A temperature ramp rate of 15 °C/s was used for samples annealed in an *ex situ* RTA chamber.

For studies involving samples that were not intentionally oxidized, a pressurized Ar glovebag adjacent to the rapid thermal nanowire growth chamber was used to prepare samples for XPS measurements after growth. During the transfer process, nonemergency lighting was turned off in the room to minimize exposure to UV light from the fluorescent lamps in the room.[42] After samples were attached to the XPS holder within the Ar glovebag, the holder was placed in a light-tight vacuum transfer vessel, which was pumped down to less than 10 mTorr before being brought to the XPS. Transfer from the growth chamber to the load-lock of the XPS was completed in less than 30 min for these samples. Of these samples, those that were annealed in vacuum in the growth chamber were annealed within approximately 2 min after the end of growth, after exhausting and flushing the growth atmosphere from the chamber. $Ge_{1-x}Sn_x$ samples that were annealed in H_2 were held in an argon-pressurized load lock above atmospheric pressure, while gaseous hydrochloric acid and H_2 were flushed for 4.5 h through the source gas lines of the rapid thermal CVD chamber. These lines were heated to 70 °C, to remove any Sn contamination prior to high temperature annealing. This same decontamination procedure was used between subsequent $Ge_{1-x}Sn_x$ growths as well, in an effort to improve sample reproducibility.

Quantification of the XPS spectra was performed using a Shirley background and two different peak models built upon the Gaussian line shape and the Lorentzian line shape. The oxide components were fitted using a symmetric pseudo-Voigt function. Elemental components were fitted with a Finite Lorentzian (LF) function[43] to account for the expected asymmetry of the Ge and Sn peaks.[44] The LF function was chosen as an improvement over the Doniach-Sunjic asymmetric line shape to prevent incorrect incorporation of peak area from binding energies far above the center of the peak profile.[45,46] Further information regarding the lineshapes used is provided in the Supporting Information.

Vertical nanowire cross-sections, defined here as cutting along the growth axis with the nanowire still attached to the growth substrate as shown in Figure S1(a,b), were also prepared. Vertical cross-sections utilized electron beam carbon depositions at multiple angles to better coat the sidewalls of the nanowire to protect from amorphization from direct ion beam exposure as well as from ejected material during the various preparation steps. Transmission electron microscopy was performed in an FEI Titan at 300 kV as well as in collaboration with ThermoFisher using a Themis at 300 kV with an aberration corrector for the probe forming optics for horizontal cross-section samples and a Talos F200X G2 at 200 kV. Energy dispersive X-ray spectroscopy (EDS) was performed in STEM mode using a SuperX EDS detector on both the Themis and Talos.

IN SITU DECOMPOSITION OF NATIVE GESN OXIDE

Investigations of the thermal stability of the native GeSn oxide were performed using samples previously grown[41] and purposefully left to oxidize at room temperature in laboratory air. Samples were left to oxidize for at least 2 months to

https://doi.org/10.1021/acsaelm.2c01061
ACS Appl. Electron. Mater. 2022, 4, 5406−5412

minimize sample-to-sample variation in oxide thickness.[18,47] The samples investigated had Sn compositions in the GeSn shell of 2, 4, 6, and 12 at% as determined via XRD, using a procedure described previously.[41] The growth conditions for these samples are shown in Table S2. Results from *in situ* XPS annealing are shown for the 12 at% Sn sample in Figure 1 for

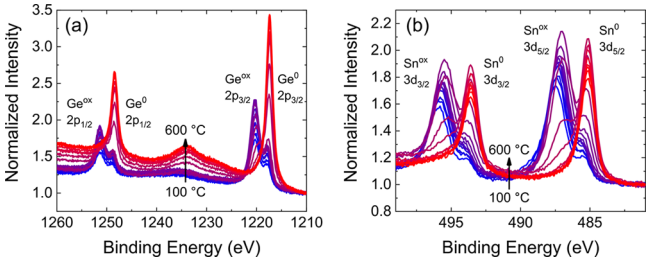

Figure 1. Temperature dependent XPS results of the Ge 2p (a) and Sn 3d (b) peaks from a 12 at% Sn core/shell Ge/$Ge_{1-x}Sn_x$ sample annealed with an *in situ* XPS hot-stage. The sample was purposefully allowed to form a native oxide prior to measurement. Nonlinear spacings were chosen to focus on the oxide decomposition; a list of temperature spacings is provided in the Supporting Information in Table S3.

both Sn 3d peaks and Ge 2p peaks. Results for the lower Sn content samples are shown in the Supporting Information. The samples were held at each temperature for 5 min while collecting the XPS spectra, followed by approximately 2 min of temperature ramp and stabilization.

Initially, the spectra show predominantly fully oxidized Sn (Sn^{ox}) and Ge (Ge^{ox}) at the surface, before decomposition of the oxide occurs at intermediate temperatures, leaving only metallic Sn (Sn^0) and Ge (Ge^0) on the surface at the highest temperatures. During the decomposition of the oxides, the peak energy shifts to intermediate values between the fully oxidized and metallic peak positions, indicating the presence of various suboxides present immediately prior to the full decomposition of the oxide. These suboxides have been documented in the formation and decomposition of pure Ge oxide previously[18,48] and play a significant role in its thermal decomposition.[12,13]

For quantitative analysis of the oxide decomposition, the Ge $2p_{1/2}$ and Sn $3d_{5/2}$ peaks were chosen. Analysis of the data in Figure 1, as well as 2, 4, and 6 at% Sn (Supporting Information), was performed via a procedure described in detail in the Supporting Information. To quantify the decomposition of the GeSn oxide, the oxidation percentage of both Sn and Ge in the sample volume sampled by XPS were calculated as,

$$Oxidation\% = 100\left[\frac{E^{ox}}{E^{ox} + E^{0}}\right] \quad (1)$$

where E^{ox} is the computed composition of the dioxide of a given component compared to the dioxide and elemental components of both Ge and Sn, and E^0 is similarly the composition of the element of a given component. The oxidation percentage results are plotted in Figure 2(a) for both Ge and Sn. A characteristic oxide decomposition temperature, T_o which corresponds to the maximum rate of change of oxidation of the surface, was defined using a logistic fitting function,

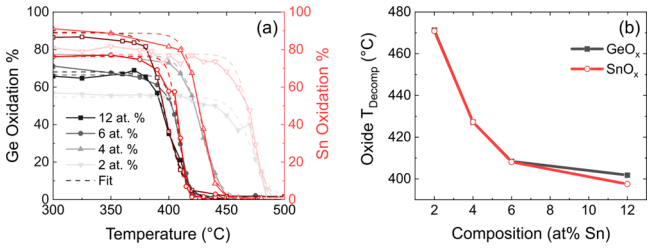

Figure 2. Oxidation percentage of Ge (black) and Sn (red) as a function of annealing temperature (a) derived from Figure 1 for core/shell Ge/GeSn nanowires of Sn contents from 2 to 12 at% via XPS. Results from fitting via eq 2 to determine the oxidation decomposition temperature as a function of Sn content (b) for the same samples as (a).

$$Oxidation\%(T) = \frac{a}{1 + e^{-k(T-T_o)}} \quad (2)$$

where k and a are fitting constants. This definition of the oxide decomposition temperature is consistent with that used to analyze data obtained from thermal desorption spectroscopy (TDS), where the peak in TDS corresponds to the greatest amount of material released in each measurement period, i.e., the greatest rate of change of material on the surface.[12]

The oxide decomposition temperature is plotted as a function of the XRD measured Sn content of the sample in Figure 2(b). The discrepancy at the highest Sn composition likely arises due to slight variations in the fitting results for the data in Figure 1, causing a shift in the fitting of eq 2, although a real sample effect due to the higher Sn content cannot be ruled out. Throughout the rest of the range, the decomposition temperatures for both the Ge oxide and Sn oxide components are found to lie at nearly identical temperatures and decrease monotonically with increasing Sn content. The simultaneous decomposition of both oxides implies a uniformly mixed GeSn oxide, rather than a phase separated oxide with chemically distinct domains that would be expected to decompose at different temperatures.

SURFACE MORPHOLOGY AND COMPOSITION EVOLUTION AFTER RAPID THERMAL ANNEALING

Investigation of the surface chemical composition of $Ge_{1-x}Sn_x$ was performed using *ex situ* rapid thermal annealing prior to XPS analysis to enable more precise definitions of thermal budgets. $Ge_{1-x}Sn_x$ shells were grown at 275 °C with P_{GeH_4} = 0.22 Torr and P_{SnCl_4} = 0.2 Torr resulting in shells with 10 at% Sn. Typical XRD patterns are shown in Figure S7. Due to the transfer process and handling, a small amount of adventitious C was measurable on these *ex situ* annealed samples, enabling charge compensation by setting the C 1s peak position to 284.8 eV for all measurements.[46]

I. H_2 Annealing. Hydrogen annealing of $Ge_{1-x}Sn_x$ was explored as it has shown the ability to passivate deep level recombination centers.[49] Additionally, H_2 annealing creates a reducing atmosphere in effort of analyzing an oxide free surface of GeSn. Results for seven samples annealed in 30 Torr H_2 under different thermal conditions, as well as a room temperature control, are shown in Figure 3. Data in Figure 3 have been shifted along the intensity axis for clarity in peak shape; unshifted data is shown in Figure S8. The Ge peak intensity monotonically decreases with increasing thermal annealing budget, while the Sn peak intensity increases and

https://doi.org/10.1021/acsaelm.2c01061
ACS Appl. Electron. Mater. 2022, 4, 5406−5412

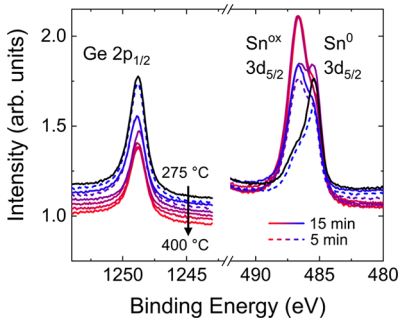

Figure 3. XPS results from *ex situ* H_2 RTA of core/shell Ge/GeSn nanowires with 10 at% Sn. Black line indicates room temperature control sample; temperature increases from 275 to 400 °C from blue to red and are the same as in Figure 6. Dashed lines indicate 5 min anneals; solid lines indicate 15 min anneals. The plotted curves have been offset vertically from each other to visualize changes to the shape of the peaks more easily.

shows greater intensity in the oxidized shoulder component at higher binding energies. All samples showed no measurable oxidation of the Ge peak, while the Sn peak exhibited an oxide component for all measurements. Previous reports demonstrate clear XPS detection of Sn oxidation with just 1000 L (1 L = 10^{-6} Torr·s) of O_2 exposure at room temperature.[50,51] Thus, the small Sn oxide shoulder observed from the control sample is likely due to inherent low level leaks after growth, during sample transfer, and Ar glovebag preparation prior to XPS measurements.

The large increase in Sn signal relative to Ge in Figure 3 is indicative of Sn segregation to the GeSn surface, which occurs simultaneously with the morphological changes observed in the SEM images of Figure 4. Annealing under H_2 for 15 min at 325 °C, as shown in Figure 4(b), results in dramatic surface morphology changes. As we have reported previously[39] for air-exposed samples that had been deposited under Sn-excess conditions, the prominent, spherically shaped regions, typically

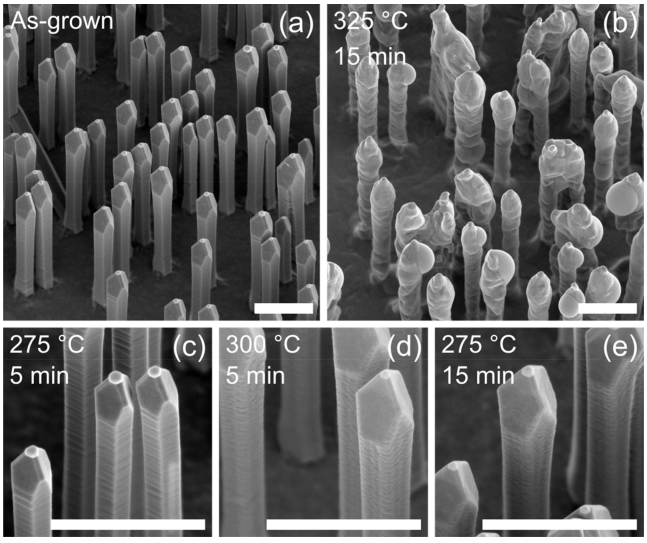

Figure 4. Comparison of as-grown (a) and multiple H_2 anneal conditions performed in the rapid thermal growth chamber for core/shell Ge/GeSn nanowires with 10 at% Sn. H_2 annealing conditions shown are (b) 325 °C for 15 min, (c) 275 °C for 5 min, (d) 300 °C for 5 min, and (e) 275 °C for 15 min. Images taken at 30° tilt, and scale bars are 1 μm.

near the tips of the nanowires, coincide with areas of fully oxidized Sn. The loss of faceting on the nanowire sidewalls compared to Figure 4(a) is also seen in samples with excess Sn on the surface. A change in the nanowire sidewall morphology is seen for all thermal budgets exceeding 275 °C for 5 min under 30 Torr of H_2, as shown in Figure 4(b,d,e).

A sample with similar morphology to that seen in Figure 4(b) was lifted out as a vertical FIB cross-section and analyzed via STEM EDS mapping, the results of which are shown in Figure 5. The bright ellipsoidal regions on the left side of the

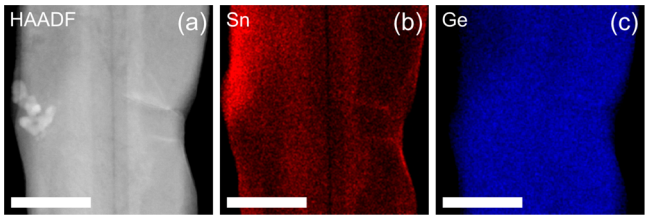

Figure 5. Vertical cross-section HAADF STEM image (a) and STEM EDS composition maps of Sn (b) and Ge (c) of a defective core/shell Ge/GeSn nanowire with morphology similar to that in Figure 4(b). The position of the core Ge nanowire is seen as a darker gray vertical rectangular section in the HAADF image with a width of 45 nm. Scale bars are 100 nm.

HAADF image are Au (EDS map not shown), indicating diffusion from the tip of the nanowire. In the STEM EDS map of this defective shell sample, we find an inhomogeneous distribution of Sn, including regions of tin enrichment evident near the wire surface. Away from the Sn-enriched surface regions, there are many regions within the shell that are Sn-deficient both in the field of view shown in Figure 5 and elsewhere along the length of the nanowire. The regions of locally enhanced Sn composition near the $Ge_{1-x}Sn_x$ shell surface are consistent with the XPS results shown in Figure 4.

Quantitative analysis of the XPS data in Figure 3 is performed using the fitting procedures described in the Methods section. An expression similar to that in eq 1 is used to find the relative percentage of Sn on the surface of the sample,

$$Sn_{surf}\% = 100\left[\frac{Sn^{ox} + Sn^{0}}{Sn^{ox} + Sn^{0} + Ge^{ox} + Ge^{0}}\right] \quad (3)$$

using the integrated intensities of the measured components of the Ge $2p_{1/2}$ and Sn $3d_{5/2}$ peaks. The results of the analysis of these fits are shown in Figure 6 compared to three separate control measurements of unannealed samples. Quantitative XPS analysis shows agreement with the qualitative SEM observations in Figure 4 and the STEM EDS results in Figure 5, where the surface morphology evolves away from sharp facets at higher thermal budgets exceeding 275 °C for 5 min. These microstructural observations are correlated with segregation of Sn to the surface of the samples (Figure 6).

II. Vacuum Annealing. In addition to in-chamber postgrowth annealing in a H_2 environment, postgrowth vacuum annealing was performed with a chamber pressure of approximately 50 mTorr. The results for annealing at 300 °C for 15 min under this vacuum condition are shown in Figure 7(a), compared to a control sample and H_2 annealing for the same time and temperature. Results after 275 °C for 15 min were similar and are not shown. Unlike results from H_2 annealing, the oxide shoulder on the Sn peak constitutes

https://doi.org/10.1021/acsaelm.2c01061
ACS Appl. Electron. Mater. 2022, 4, 5406−5412

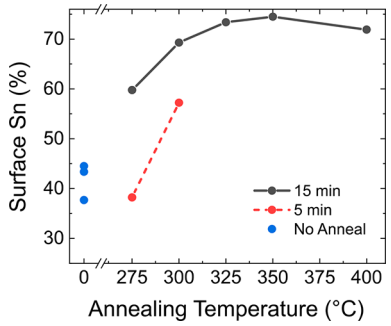

Figure 6. Calculated surface Sn percentage of H_2 annealed core/shell $Ge/Ge_{1-x}Sn_x$ nanowire samples compared to as-grown samples (blue) with 10 at% Sn for 5 and 15 min anneals. Surface Sn percentage is calculated via eq 3.

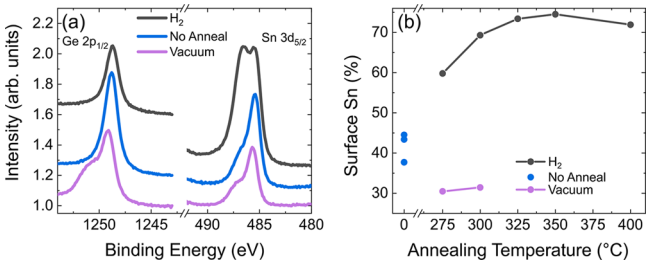

Figure 7. Comparison of XPS results from in-reactor H_2 and vacuum (~50 mTorr) RTA of core/shell $Ge/Ge_{1-x}Sn_x$ nanowires (a) with 10 at% Sn at 300 °C for 15 min. The plotted curves have been offset vertically from each other to visualize changes to the shape of the peaks more easily. Calculated surface Sn percentage (b) of 15 min in-reactor H_2 and vacuum RTA of core/shell $Ge/Ge_{1-x}Sn_x$ nanowire samples compared to as-grown samples (blue) with 10 at% Sn. Surface Sn percentage is calculated via eq 3.

approximately the same proportion of the total Sn signal. Also, Ge oxidation was observed under these conditions, unlike for in-reactor annealing under H_2 and subsequent transfer to the XPS chamber. This difference is ascribed to a small background O_2 pressure in the reactor chamber during the high temperature annealing, causing surface oxidation to occur, in contrast to the situation in the reducing H_2 environment.

Analysis of the surface Sn composition, shown in Figure 7(b), reveals a slight decrease in total Sn surface composition compared to the control samples, and a dramatic decrease compared to the H_2 annealing results. This lack of observed Sn surface segregation via XPS is again confirmed via the surface morphology observed in SEM imaging, shown in Figure 8. The vacuum annealed sample, Figure 8(b), is visually identical to the as-grown sample in Figure 4(a), with the same strong

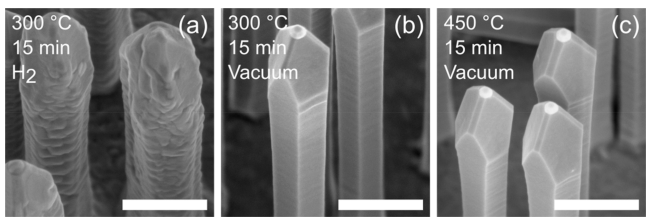

Figure 8. SEM images at 30° tilt comparing surface morphologies of core/shell $Ge/Ge_{1-x}Sn_x$ nanowire after H_2 (a) and vacuum (b) annealing for 15 min at 300 °C and vacuum annealing for 15 min at 450 °C (c). Scale bars are 500 nm.

faceting observed, unlike the H_2 annealing results above 275 °C for 5 min, as shown in Figures 4 and 8(a).

The change in surface morphology is correlated with surface Sn segregation. Previous reports of strained SiGe in both planar[52] and core/shell nanowire[53] geometries have shown a surface diffusion mediated mechanism for the development of surface undulations at elevated temperatures. Due to the low melting point of Sn (232 °C), any Sn which has segregated to the surface likely forms a liquid wetting layer, which would allow for more rapid surface diffusion.[54,55] Thus, due to a sufficient background O_2 composition during the vacuum annealing process, an *in situ* GeSn oxide is formed, as evidenced by Figure 7(a), which blocks Sn segregating to the surface and mediating the surface morphology changes seen during H_2 annealing. The success of this method has been observed in the surface morphology of GeSn nanowires annealed under vacuum at 450 °C for 15 min, shown in Figure 8 (c), which indicates successful inhibition of surface Sn segregation at temperatures 175 °C greater than under otherwise identical conditions in a H_2 ambient.

CONCLUSION

X-ray photoelectron spectroscopy was used to examine the thermal stability of the $Ge_{1-x}Sn_x$ surface as well as its native oxide on core/shell $Ge/Ge_{1-x}Sn_x$ nanowires. *In situ* ultrahigh vacuum annealing in the XPS chamber was performed on GeSn native oxide coated nanowire samples via quasistatic annealing with an average ramp rate of approximately 0.7 °C/min. Analysis of the resulting photoelectron spectra revealed that the GeSn native oxide decomposes at lower temperatures as the Sn content is increased, ranging from approximately 475 °C at 2 at% Sn to 400 °C at 12 at% Sn. Annealing was performed in the rapid thermal CVD growth chamber. Samples were not purposefully oxidized prior to annealing and were annealed under either a reducing H_2 environment or a rough (~50 mTorr) vacuum environment. Hydrogen annealing revealed a maximum thermal budget of 275 °C for 5 min before correlated observations of surface Sn segregation and surface morphology change. Rough vacuum annealing resulted in *in situ* oxidation of the GeSn surface, providing a barrier to Sn surface segregation. This prevented Sn diffusion mediated restructuring of the surface facet morphology at thermal budgets up to 450 °C for 15 min. These results indicate that formation of a thin surface oxide layer prior to or during annealing of GeSn can significantly block surface segregation of Sn under thermal processing conditions that are relevant for device fabrication.

ASSOCIATED CONTENT

Data Availability Statement

The data that support the findings of this study are available from the corresponding author upon reasonable request.

Supporting Information

The Supporting Information is available free of charge at https://pubs.acs.org/doi/10.1021/acsaelm.2c01061.

Literature summary of GeSn annealing, growth conditions, schematic figures, a description of XPS line fitting, additional annealing of oxidized GeSn nanowire samples, XRD of GeSn samples, and uncorrected XPS of *ex situ* H_2 RTA GeSn samples (PDF)

https://doi.org/10.1021/acsaelm.2c01061
ACS Appl. Electron. Mater. 2022, 4, 5406−5412

AUTHOR INFORMATION

Corresponding Author

Paul C. McIntyre − *Department of Materials Science and Engineering, Stanford University, Stanford, California 94305, United States;* orcid.org/0000-0002-7498-831X; Email: pcm1@stanford.edu

Authors

Michael R. Braun − *Department of Materials Science and Engineering, Stanford University, Stanford, California 94305, United States;* orcid.org/0000-0001-6957-1838

J. Zach Lentz − *Department of Materials Science and Engineering, Stanford University, Stanford, California 94305, United States;* orcid.org/0000-0001-5703-7312

Ishaa Bishnoi − *Department of Materials Science and Engineering, Stanford University, Stanford, California 94305, United States*

Andrew C. Meng − *Department of Materials Science and Engineering, University of Pennsylvania, Philadelphia, Pennsylvania 19104, United States;* orcid.org/0000-0002-3060-8928

Lee Casalena − *ThermoFisher Scientific, Hillsboro, Oregon 97124, United States*

Huikai Cheng − *ThermoFisher Scientific, Hillsboro, Oregon 97124, United States*

Complete contact information is available at: https://pubs.acs.org/10.1021/acsaelm.2c01061

Author Contributions

Michael R. Braun: Conceptualization (supporting), Data Curation (lead), Formal Analysis (lead), Investigation (lead), Methodology (lead), Visualization (lead), Original Draft Preparation (Lead), Review and Editing (equal). **J. Zach Lentz:** Investigation (supporting), Methodology (supporting), Review and Editing (supporting). **Ishaa Bishnoi:** Investigation (supporting), Methodology (supporting), Visualization (supporting). **Andrew C. Meng:** Investigation (supporting). **Lee Casalena:** Investigation (supporting), Resources (supporting). **Huikai Cheng:** Investigation (supporting), Resources (supporting). **Paul C. McIntyre:** Conceptualization (lead), Funding Acquisition (lead), Methodology (supporting), Resources (lead), Supervision (lead), Review and Editing (equal).

Notes

The authors declare no competing financial interest.

ACKNOWLEDGMENTS

This research was supported by the US National Science Foundation grant DMR-2003266. Part of this work was performed at the Stanford Nano Shared Facilities (SNSF), supported by the National Science Foundation under award ECCS-2026822. MRB acknowledges financial support from NSF GRFP award DGE-1656518. This material is based upon work supported by the U.S. Department of Energy, Office of Science, Office of Workforce Development for Teachers and Scientists, Office of Science Graduate Student Research (SCGSR) program. The SCGSR program is administered by the Oak Ridge Institute for Science and Education for the DOE under contract number DE-SC0014664.

REFERENCES

(1) Oka, H.; Mizubayashi, W.; Ishikawa, Y.; Uchida, N.; Mori, T.; Endo, K. Flash lamp annealing processing to improve the performance of high-Sn content GeSn n-MOSFETs. *Applied Physics Express* **2021**, *14*, 096501.

(2) Takase, R.; Ishimaru, M.; Uchida, N.; Maeda, T.; Sato, K.; Lieten, R. R.; Locquet, J.-P. Behavior of Sn atoms in GeSn thin films during thermal annealing: Ex-situ and in-situ observations. *J. Appl. Phys.* **2016**, *120*, 245304.

(3) Fournier-Lupien, J.-H.; Chagnon, D.; Levesque, P.; Almutairi, A. A.; Wirths, S.; Pippel, E.; Mussler, G.; Hartmann, J.-M.; Mantl, S.; Buca, D.; Moutanabbir, O. In Situ Studies of Germanium-Tin and Silicon-Germanium-Tin Thermal Stability. *ECS Trans.* **2014**, *64*, 903−911.

(4) Wang, L.; Wang, W.; Zhou, Q.; Pan, J.; Zhang, Z.; Tok, E. S.; Yeo, Y.-C. Post-growth annealing of germanium-tin alloys using pulsed excimer laser. *J. Appl. Phys.* **2015**, *118*, 025701.

(5) Wang, W.; Li, L.; Tok, E. S.; Yeo, Y.-C. Self-assembly of tin wires via phase transformation of heteroepitaxial germanium-tin on germanium substrate. *J. Appl. Phys.* **2015**, *117*, 225304.

(6) Wang, W.; Lei, D.; Dong, Y.; Zhang, Z.; Pan, J.; Gong, X.; Tok, E.-S.; Yeo, Y.-C. Kinetics of plasma oxidation of germanium-tin (GeSn). *Appl. Surf. Sci.* **2017**, *425*, 95−99.

(7) Pillarisetty, R. Academic and industry research progress in germanium nanodevices. *Nature* **2011**, *479*, 324−328.

(8) Magnone, P.; Crupi, F.; Alioto, M.; Kaczer, B.; De Jaeger, B. Understanding the Potential and the Limits of Germanium pMOSFETs for VLSI Circuits From Experimental Measurements. *IEEE Transactions on Very Large Scale Integration (VLSI) Systems* **2011**, *19*, 1569−1582.

(9) Gupta, S., Chen, R., Magyari-Kope, B., Lin, H., Yang, B., Nainani, A., Nishi, Y., Harris, J. S.; Saraswat, K. C. GeSn technology: Extending the Ge electronics roadmap. *2011 International Electron Devices Meeting*, **2011**, 16.16.1−16.16.4.

(10) Molle, A.; Bhuiyan, M. N. K.; Tallarida, G.; Fanciulli, M. Formation and stability of germanium oxide induced by atomic oxygen exposure. *Materials Science in Semiconductor Processing* **2006**, *9*, 673−678.

(11) Prabhakaran, K.; Maeda, F.; Watanabe, Y.; Ogino, T. Distinctly different thermal decomposition pathways of ultrathin oxide layer on Ge and Si surfaces. *Appl. Phys. Lett.* **2000**, *76*, 2244−2246.

(12) Wang, S. K.; Kita, K.; Lee, C. H.; Tabata, T.; Nishimura, T.; Nagashio, K.; Toriumi, A. Desorption kinetics of GeO from GeO_2/Ge structure. *J. Appl. Phys.* **2010**, *108*, 054104.

(13) Kai Wang, S.; Liu, H.-G.; Toriumi, A. Kinetic study of GeO disproportionation into a GeO_2/Ge system using x-ray photoelectron spectroscopy. *Appl. Phys. Lett.* **2012**, *101*, 061907.

(14) Wang, X.; Nishimura, T.; Yajima, T.; Toriumi, A. Thermal oxidation kinetics of germanium. *Appl. Phys. Lett.* **2017**, *111*, 052101.

(15) Wang, X.; Zhao, Z.; Xiang, J.; Wang, W.; Zhang, J.; Zhao, C.; Ye, T. Experimental investigation on oxidation kinetics of germanium by ozone. *Appl. Surf. Sci.* **2016**, *390*, 472−480.

(16) Kotera, Y.; Yonemura, M. Kinetics of the transformation of germanium oxide. *Trans. Faraday Soc.* **1963**, *59*, 147−155.

(17) Bernstein, R. B.; Cubicciotti, D. The kinetics of the reaction of germanium and oxygen. *J. Am. Chem. Soc.* **1951**, *73*, 4112−4114.

(18) Tabet, N. A.; Salim, M. A.; Al-Oteibi, A. L. XPS study of the growth kinetics of thin films obtained by thermal oxidation of germanium substrates. *J. Electron Spectrosc. Relat. Phenom.* **1999**, *101*−*103*, 233−238.

(19) Kato, K.; Taoka, N.; Asano, T.; Yoshida, T.; Sakashita, M.; Nakatsuka, O.; Zaima, S. Formation of high-quality oxide/$Ge_{1-x}Sn_x$ interface with high surface Sn content by controlling Sn migration. *Appl. Phys. Lett.* **2014**, *105*, 122103.

(20) Claeys, C.; Simoen, E. *Germanium-Based Technologies: From Materials to Devices*; Elsevier, 2007.

(21) Assali, S.; Elsayed, M.; Nicolas, J.; Liedke, M. O.; Wagner, A.; Butterling, M.; Krause-Rehberg, R.; Moutanabbir, O. Vacancy

complexes in nonequilibrium germanium-tin semiconductors. *Appl. Phys. Lett.* **2019**, *114*, 251907.
(22) Slotte, J.; Rummukainen, M.; Tuomisto, F.; Markevich, V. P.; Peaker, A. R.; Jeynes, C.; Gwilliam, R. M. Evolution of vacancy-related defects upon annealing of ion-implanted germanium. *Phys. Rev. B* **2008**, *78*, 085202.
(23) Nakatsuka, O.; Tsutsui, N.; Shimura, Y.; Takeuchi, S.; Sakai, A.; Zaima, S. Mobility Behavior of $Ge_{1-x}Sn_x$Layers Grown on Silicon-on-Insulator Substrates. *Jpn. J. Appl. Phys.* **2010**, *49*, 04DA10.
(24) Weber, J.; Hiller, M.; Lavrov, E. V. Hydrogen in germanium. *Materials Science in Semiconductor Processing* **2006**, *9*, 564−570.
(25) Kim, J.-H.; Lee, Y.-H.; Park, J.-H.; Lee, B.-J.; Byeon, Y.-W.; Lee, J.-C. Ultrafast Na Transport into Crystalline Sn via Dislocation-Pipe Diffusion. *Small* **2022**, *18*, 2104944.
(26) Volin, T. E.; Lie, K. H.; Balluffi, R. W. Measurement of rapid mass transport along individual dislocations in aluminum. *Acta Metall.* **1971**, *19*, 263−274.
(27) Bhargava, N.; Gupta, J. P.; Faleev, N.; Wielunski, L.; Kolodzey, J. Thermal Stability of Annealed Germanium-Tin Alloys Grown by Molecular Beam Epitaxy. *J. Electron. Mater.* **2017**, *46*, 1620−1627.
(28) Zhang, X.; Zhang, D.; Cheng, B.; Liu, Z.; Zhang, G.; Xue, C.; Wang, Q. Crystal Quality Improvement of GeSn Alloys by Thermal Annealing. *ECS Solid State Letters* **2014**, *3*, P127−P130.
(29) Jia, H.; Jurczak, P.; Yang, J.; Tang, M.; Li, K.; Deng, H.; Dang, M.; Chen, S.; Liu, H. Impact of ex-situ annealing on strain and composition of MBE grown GeSn. *J. Phys. D: Appl. Phys.* **2020**, *53*, 485104.
(30) Zaumseil, P.; Hou, Y.; Schubert, M. A.; von den Driesch, N.; Stange, D.; Rainko, D.; Virgilio, M.; Buca, D.; Capellini, G. The thermal stability of epitaxial GeSn layers. *APL Materials* **2018**, *6*, 076108.
(31) Wang, W.; Dong, Y.; Zhou, Q.; Tok, E. S.; Yeo, Y.-C. Germanium−tin interdiffusion in strained Ge/GeSn multiple-quantum-well structure. *J. Phys. D: Appl. Phys.* **2016**, *49*, 225102.
(32) Zhang, Z. P.; Song, Y. X.; Li, Y. Y.; Wu, X. Y.; Zhu, Z. Y. S.; Han, Y.; Zhang, L. Y.; Huang, H.; Wang, S. M. Effect of thermal annealing on structural properties of GeSn thin films grown by molecular beam epitaxy. *AIP Advances* **2017**, *7*, 105020.
(33) Wang, L.; Zhang, Y.; Wu, Y.; Liu, T.; Miao, Y.; Meng, L.; Jiang, Z.; Hu, H. Effects of Annealing on the Behavior of Sn in GeSn Alloy and GeSn-Based Photodetectors. *IEEE Trans. Electron Devices* **2020**, *67*, 3229−3234.
(34) Comrie, C. M.; Mtshali, C. B.; Sechogela, P. T.; Santos, N. M.; van Stiphout, K.; Loo, R.; Vandervorst, W.; Vantomme, A. Interplay between relaxation and Sn segregation during thermal annealing of GeSn strained layers. *J. Appl. Phys.* **2016**, *120*, 145303.
(35) Lei, D.; Lee, K. H.; Bao, S.; Wang, W.; Masudy-Panah, S.; Tan, C. S.; Tok, E. S.; Gong, X.; Yeo, Y.-C. Thermal stability of germanium-tin (GeSn) fins. *Appl. Phys. Lett.* **2017**, *111*, 252103.
(36) Li, H.; Cui, Y. X.; Wu, K. Y.; Tseng, W. K.; Cheng, H. H.; Chen, H. Strain relaxation and Sn segregation in GeSn epilayers under thermal treatment. *Appl. Phys. Lett.* **2013**, *102*, 251907.
(37) Meng, A. C.; Braun, M. R.; Wang, Y.; Fenrich, C. S.; Xue, M.; Diercks, D. R.; Gorman, B. P.; Richard, M. I.; Marshall, A. F.; Cai, W.; Harris, J. S.; McIntyre, P. C. Coupling of coherent misfit strain and composition distributions in core−shell $Ge/Ge_{1-x}Sn_x$ nanowire light emitters. *Materials Today Nano* **2019**, *5*, 100026.
(38) Zangenberg, N. R.; Lundsgaard Hansen, J.; Fage-Pedersen, J.; Nylandsted Larsen, A. Ge Self-Diffusion in Epitaxial $Si_{1-x}Ge_x$ Layers. *Phys. Rev. Lett.* **2001**, *87*, 125901.
(39) Meng, A. C.; Wang, Y.; Braun, M. R.; Lentz, J. Z.; Peng, S.; Cheng, H.; Marshall, A. F.; Cai, W.; McIntyre, P. C. Bending and precipitate formation mechanisms in epitaxial Ge-core/GeSn-shell nanowires. *Nanoscale* **2021**, *13*, 17547−17555.
(40) Meng, A. C.; Fenrich, C. S.; Braun, M. R.; McVittie, J. P.; Marshall, A. F.; Harris, J. S.; McIntyre, P. C. Core-Shell Germanium/Germanium−Tin Nanowires Exhibiting Room-Temperature Direct- and Indirect-Gap Photoluminescence. *Nano Lett.* **2016**, *16*, 7521−7529.
(41) Meng, A. C.; Braun, M. R.; Wang, Y.; Peng, S.; Tan, W.; Lentz, J. Z.; Xue, M.; Pakzad, A.; Marshall, A. F.; Harris, J. S.; Cai, W.; McIntyre, P. C. Growth mode control for direct-gap core/shell Ge/GeSn nanowire light emission. *Mater. Today* **2020**, *40*, 101−113.
(42) Adhikari, H.; McIntyre, P. C.; Sun, S.; Pianetta, P.; Chidsey, C. E. D. Photoemission studies of passivation of germanium nanowires. *Appl. Phys. Lett.* **2005**, *87*, 263109.
(43) Major, G. H.; Shah, D.; Avval, T. G.; Fernandez, V.; Fairley, N.; Linford, M. R. Advanced Line Shapes in X-Ray Photoelectron Spectroscopy II. *Vac. Technol. Coat.* **2020**, *21*, 35−39.
(44) Doniach, S.; Sunjic, M. Many-electron singularity in X-ray photoemission and X-ray line spectra from metals. *Journal of Physics C: Solid State Physics* **1970**, *3*, 285−291.
(45) Biesinger, M. C.; Payne, B. P.; Lau, L. W. M.; Gerson, A.; Smart, R. S. C. X-ray photoelectron spectroscopic chemical state quantification of mixed nickel metal, oxide and hydroxide systems. *Surf. Interface Anal.* **2009**, *41*, 324−332.
(46) Gengenbach, T. R.; Major, G. H.; Linford, M. R.; Easton, C. D. Practical guides for x-ray photoelectron spectroscopy (XPS): Interpreting the carbon 1s spectrum. *Journal of Vacuum Science & Technology A* **2021**, *39*, 013204.
(47) Tabet, N.; Al-Sadah, J.; Salim, M. GROWTH OF OXIDE LAYER ON GERMANIUM (011) SUBSTRATE UNDER DRY AND WET ATMOSPHERES. *Surf. Rev. Lett.* **1999**, *06*, 1053−1060.
(48) Schmeisser, D.; Schnell, R. D.; Bogen, A.; Himpsel, F. J.; Rieger, D.; Landgren, G.; Morar, J. F. Surface oxidation states of germanium. *Surf. Sci.* **1986**, *172*, 455−465.
(49) Pearton, S. J.; Kahn, J. M.; Hansen, W. L.; Haller, E. E. Deuterium in germanium: Interaction with point defects. *J. Appl. Phys.* **1984**, *55*, 1464−1471.
(50) Lee, A. F.; Lambert, R. M. Oxidation of Sn overlayers and the structure and stability of Sn oxide films on Pd(111). *Phys. Rev. B* **1998**, *58*, 4156−4165.
(51) Asbury, D. A.; Hoflund, G. B. A surface study of the oxidation of polycrystalline tin. *Journal of Vacuum Science & Technology A* **1987**, *5*, 1132−1135.
(52) Dutartre, D.; Warren, P.; Chollet, F.; Gisbert, F.; Bérenguer, M.; Berbézier, I. Defect-free Stranski-Krastanov growth of strained $Si_{1-x}Ge_x$ layers on Si. *J. Cryst. Growth* **1994**, *142*, 78−86.
(53) Hu, S.; Kawamura, Y.; Huang, K. C. Y.; Li, Y.; Marshall, A. F.; Itoh, K. M.; Brongersma, M. L.; Mcintyre, P. C. Thermal Stability and Surface Passivation of Ge Nanowires Coated by Epitaxial SiGe Shells. *Nano Lett.* **2012**, *12*, 1385−1391.
(54) Misra, S.; Yu, L.; Chen, W.; Roca i Cabarrocas, P. Wetting Layer: The Key Player in Plasma-Assisted Silicon Nanowire Growth Mediated by Tin. *J. Phys. Chem. C* **2013**, *117*, 17786−17790.
(55) Yu, L.; Fortuna, F.; O'Donnell, B.; Patriache, G.; Roca i Cabarrocas, P. Stability and evolution of low-surface-tension metal catalyzed growth of silicon nanowires. *Appl. Phys. Lett.* **2011**, *98*, 123113.

https://doi.org/10.1021/acsaelm.2c01061
ACS Appl. Electron. Mater. 2022, 4, 5406−5412